3D tensor factorization approach to single-frame model-free blind-image deconvolution

Ivica Kopriva

Division of Laser and Atomic Research and Development, Ruđer Bošković Institute, Bijenička cesta 54, HR-10000, Zagreb, Croatia (ikopriva@gmail.com)

Received March 31, 2009; revised June 4, 2009; accepted June 4, 2009;
posted July 9, 2009 (Doc. ID 109499); published September 14, 2009

By applying a bank of 2D Gabor filters to a blurred image, single-frame blind-image deconvolution (SF BID) is formulated as a 3D tensor factorization (TF) problem, with the key contribution that neither origin nor size of the spatially invariant blurring kernel is required to be known or estimated. Mixing matrix, the original image, and its spatial derivatives are identified from the factors in the Tucker3 model of the multichannel version of the blurred image. Previous approaches to 2D Gabor-filter-bank-based SF BID relied on 2D representation of the multichannel version of the blurred image and matrix factorization methods such as nonnegative matrix factorization (NMF) and independent component analysis (ICA). Unlike matrix factorization-based methods 3D TF preserves local structure in the image. Moreover, 3D TF based on the PARAFAC model is unique up to permutation and scales under very mild conditions. To achieve this, NMF and ICA respectively require enforcement of sparseness and statistical independence constraints on the original image and its spatial derivatives. These constraints are generally not satisfied. The 3D TF-based SF BID method is demonstrated on an experimental defocused red–green–blue image.

OCIS codes: 100.1830, 100.3010, 100.3190, 100.6640, 100.6890.

The purpose of blind image deconvolution (BID) is to reconstruct the original image from an observation degraded by spatially invariant blurring process and noise. Neglecting the noise term, the process is modeled as a convolution of a point spread function (PSF) $\mathbf{H}(s,t)$ with an original source image $\mathbf{F}(i_1,i_2)$ as

$$\mathbf{G}(i_1,i_2)=\sum_{s=-M}^{M}\sum_{t=-M}^{M}\mathbf{H}(s,t)\mathbf{F}(i_1-s,i_2-t), \tag{1}$$

where M denotes the PSF support size and $\mathbf{G},\mathbf{F}\in\mathbb{R}_{0+}^{I_1\times I_2}$. If PSF is known, a number of algorithms are available to reconstruct original image $\mathbf{F}$ [1]. When PSF is not available, BID algorithms are important [2,3]. BID methods can be divided into those that estimate the blurring kernel $\mathbf{H}$ first and then restore the original image by some of the nonblind methods [1], and those that estimate the original image $\mathbf{F}$ and blurring kernel simultaneously. To estimate the blurring kernel a support size has to either be given or estimated. Also, quite often *a priori* knowledge about the nature of the blurring process is assumed to be available in order to use appropriate parametric model of the blurring process [2]. That is not always fulfilled in practice. Multivariate data-analysis methods such as nonnegative matrix factorization (NMF) [4] and independent component analysis (ICA) [5–7] can be used to solve a BID problem as a blind source separation problem, where an unknown blurring process is absorbed into a mixing matrix. To realize a multichannel version of the blurred image, an approach based on a bank of 2D Gabor filters was proposed in [8]. It was been the basis of the single frame (SF) BID algorithms in [4,6]. The key insight in [8] was that original image $\mathbf{F}(i_1-s,i_2-t)$ can be approximated by Taylor series expansion around $\mathbf{F}(i_1,i_2)$, giving $\mathbf{F}(i_1-s,i_2-t)=\mathbf{F}(i_1,i_2)-s\mathbf{F}_{i_1}(i_1,i_2)-t\mathbf{F}_{i_2}(i_1,i_2)-\ldots$, which enables us to rewrite Eq. (1) as

$$\mathbf{G}(i_1,i_2)=a_1\mathbf{F}(i_1,i_2)+a_2\mathbf{F}_{i_1}(i_1,i_2)+a_3\mathbf{F}_{i_2}(i_1,i_2)+\ldots, \tag{2}$$

where $a_1=\sum_{s=-M}^{M}\sum_{t=-M}^{M}\mathbf{H}(s,t)$, $a_2=-\sum_{s=-M}^{M}\sum_{t=-M}^{M}s\mathbf{H}(s,t)$, and $a_3=-\sum_{s=-M}^{M}\sum_{t=-M}^{M}t\mathbf{H}(s,t)$, and $\mathbf{F}_{i_1}$ and $\mathbf{F}_{i_2}$ are spatial derivatives in the i_1 and i_2 directions, respectively. When Gabor filters are applied on a blurred image, a new set of observed images is obtained as

$$\mathbf{G}_{i_3}(i_1,i_2)=a_{i_3,1}\mathbf{F}(i_1,i_2)+a_{i_3,2}\mathbf{F}_{i_1}(i_1,i_2)+a_{i_3,3}\mathbf{F}_{i_2}(i_1,i_2)+\ldots,\quad i_3=2,\ldots,I_3, \tag{3}$$

where $a_{i_3,1}=\sum_{s=-M}^{M}\sum_{t=-M}^{M}\mathbf{H}'_{i_3}(s,t)$, $a_{i_3,2}=-\sum_{s=-M}^{M}\times\sum_{t=-M}^{M}s\mathbf{H}'_{i_3}(s,t)$, $a_{i_3,3}=-\sum_{s=-M}^{M}\sum_{t=-M}^{M}t\mathbf{H}'_{i_3}(s,t)$, where $\mathbf{H}'_{i_3}(s,t)$ represents convolution of the appropriate i_3th Gabor filter with $\mathbf{H}(s,t)$. In the to-be-reported experiment, I have used a bank of 2D Gabor filters with two spatial frequencies and four orientations, whereas real and imaginary parts of the 2D Gabor filters were used as separate filters. Thus overall a multichannel version of the blurred image consisted of $I_3=17$ images. We refer to [4,6] for a more-detailed description of the 2D Gabor filter bank. In my previous contributions [4,6] a multichannel version of the blurred image $\mathbf{G}$ was represented in 2D as $\mathbf{G}_{(3)}\in\mathbb{R}^{I_3\times I_1 I_2}$, i.e., $\mathbf{G}_{(3)}$, was a set of I_3 images of the size $I_1\times I_2$ pixels, where the first image corresponded with the vectorized blurred image $\mathbf{G}$ and the rest of the I_3 images corresponded to vectorized images obtained after filtering the blurred image with 2D Gabor filters. In this Letter I represent a multichannel version of the blurred image as a three-way array or a 3D tensor $\underline{\mathbf{G}}\in\mathbb{R}^{I_1\times I_2\times I_3}$ with elements $g_{i_1 i_2 i_3}$, where $i_1=1,\ldots,I_1$, $i_2=1,\ldots,I_2$, and $i_3=1,\ldots,I_3$. Each index is called the way or mode, and the number of levels on one mode is called the dimension of that mode.

0146-9592/09/182835-3/$15.00

Two ways of $\underline{\mathbf{G}}$ are for rows and columns, and one way is for image index. This is standard notation adopted for use in multiway analysis [9]. 2D representation of the multichannel blurred image has two disadvantages: (i) the 3D tensor $\underline{\mathbf{G}}$ has to be mapped through three-mode flattening, also called unfolding and matricization, to matrix $\mathbf{G}_{(3)}$, whereas the local structure of the image is lost; and (ii) matrix factorization $\mathbf{G}_{(3)}=\mathbf{A}\mathbf{F}_{(3)}$ employed by linear mixing models (2) and (3) suffers from indeterminacies, because $\mathbf{A}\mathbf{T}\mathbf{T}^{-1}\mathbf{F}_{(3)}=\mathbf{G}_{(3)}$ for any invertible $\mathbf{T}$. It implies that infinitely many $(\mathbf{A}, \mathbf{F}_{(3)})$ pairs can give rise to $\mathbf{G}_{(3)}$. In my notation J rows of $\mathbf{F}_{(3)}$ represent a vectorized version of the original image $\mathbf{F}$ and its spatial derivatives, i.e., $\mathbf{F}_{(3)} \in \mathbb{R}^{J\times I_1 I_2}$. J represents an unknown number of latent variables (the original image and its spatial derivatives) in the linear mixture models (2) and (3). Meaningful solution of the factorization of $\mathbf{G}_{(3)}$ is characterized with $\mathbf{T}=\mathbf{P}\mathbf{\Lambda}$, where $\mathbf{P}$ is the permutation matrix and $\mathbf{\Lambda}$ is the diagonal matrix. These standard blind decomposition indeterminacies are obtained by imposing sparseness constraints on $\mathbf{F}_{(3)}$ by NMF algorithms [4] and statistical independence constraints by ICA algorithms [6]. Sparseness constraints imply that original image $\mathbf{F}$ and its spatial derivatives $\mathbf{F}_{i_1}$, $\mathbf{F}_{i_2}$, etc. do not occupy the same pixel, and that is generally not true. Statistical independence assumption is also not true, as already observed in [4,6,7]. To improve statistical independence between the original image and its spatial derivatives, I have used in [6] wavelet-packet-based transform to find out the narrow subband where latent variables are least dependent. Owing to this further convolution (multiscale filtering), as correctly observed in [7], many more terms in Taylor series expansion are required to get good reconstruction than when no filtering is used. When using a 3D TF approach to BID no such complications arise, because no constraints on latent variables need to be imposed in order to achieve unique factorization. For the purpose of blind decomposition of the multichannel image tensor $\underline{\mathbf{G}}$ we adopt the Tucker3 model [10],

$$\underline{\mathbf{G}} \approx \underline{\mathbf{R}}\times_1\mathbf{A}^{(1)}\times_2\mathbf{A}^{(2)}\times_3\mathbf{A}^{(3)}, \tag{4}$$

where $\underline{\mathbf{R}} \in \mathbb{R}^{J_1\times J_2\times J_3}$ is the core tensor, $\{\mathbf{A}^{(n)} \in \mathbb{R}^{I_n\times J_n}\}_{n=1}^{3}$ are factors, and $\times_n$ denotes the n-mode product of a tensor with a matrix $\mathbf{A}^{(n)}$. The result of $\underline{\mathbf{R}}\times_n\mathbf{A}^{(n)}$ is a tensor of the same order as $\underline{\mathbf{R}}$ but with the size J_n replaced by I_n. The PARAFAC model [11], also called CANDECOMP [12], is a special case of Tucker3 model when $\underline{\mathbf{R}}$ is a superdiagonal tensor with all elements zero, except those for which all indices are the same. Compared to PARAFAC, the Tucker3 model is more flexible because of the core tensor, which allows interaction of a factor with any factor in the other modes [13]. In the PARAFAC model factors in different modes can interact only factorwise. However, this restriction enables uniqueness of tensor factorization based the PARAFAC model within the permutation and scaling indeterminacies of the factors under very mild conditions [14,15]. There is no need to impose constraints on them, such as sparseness or statistical independence. Assuming that $J_1=J_2=J_3=J$ and $J\leqslant I_3$, the uniqueness condition is reduced to $k_{\mathbf{A}^{(1)}}+k_{\mathbf{A}^{(2)}}+k_{\mathbf{A}^{(3)}}\geqslant 2J+3$, where $k_{\mathbf{A}^{(n)}}$ is Kruskal rank of factor $\mathbf{A}^{(n)}$ [14,15]. Because of interaction between the factors there is no such theoretical guarantee on the uniqueness of tensor factorization based on the Tucker3 model. However, despite this the Tucker3 model has been used successfully in hyperspectral image analysis for dimensionality reduction, denoising, and target detection [16,17]. To identify the original image and its spatial derivatives, we refer to linear mixture model used in Eqs. (2) and (3),

$$\mathbf{G}_{(3)} \approx \mathbf{A}\mathbf{F}_{(3)}, \tag{5}$$

where columns of $\mathbf{A} \in \mathbb{R}^{I_3\times J}$ represent the weighting coefficients of the J images resident in the multichannel image $\mathbf{G}_{(3)}$, while rows of $\mathbf{F}_{(3)} \in \mathbb{R}^{J\times I_1 I_2}$ represent vectorized versions of the original image and its spatial derivatives. Without constraints there are infinitely many decompositions satisfying model in expression (5). From the Tucker3 model (4) and the linear mixture model (5) the matrix of weighting coefficients and the tensor of the source image and its spatial derivatives $\underline{\mathbf{F}}$ are identified as

$$\mathbf{A} \approx \mathbf{A}^{(3)},$$

$$\underline{\mathbf{F}} \approx \underline{\mathbf{R}}\times_1\mathbf{A}^{(1)}\times_2\mathbf{A}^{(2)} \approx \underline{\mathbf{G}}\times_3(\mathbf{A}^{(3)})^{\dagger}, \tag{6}$$

where $\underline{\mathbf{F}} \in \mathbb{R}^{I_1\times I_2\times J}$ and $\dagger$ denotes the Moore–Penrose pseudoinverse. What remains after three-mode multiplication of the image tensor $\underline{\mathbf{G}}$ with pseudoinverse of array factor $\mathbf{A}^{(3)}$ is first part of expression (6). According to expression (5) this must be $\underline{\mathbf{F}}$. The second part of expression (6) is much less sensitive on numerical errors, owing to the fact that only one reconstructed quantity, array factor $\mathbf{A}^{(3)}$, takes places in the reconstruction of $\underline{\mathbf{F}}$. This completes derivation of the 3D tensor factorization (TF) based SF BID algorithm that is defined without using any *a priori* information about the blurring process or source image. To estimate array factor $\mathbf{A}^{(3)}$ from image tensor $\underline{\mathbf{G}}$ based on the Tucker3 model [expression (4)] I have used the TUCKER_ALS function made available as a part of MATLAB Tensor Toolbox [18]. $\underline{\mathbf{F}}$ is then reconstructed through three-mode multiplication of the image tensor $\underline{\mathbf{G}}$ and the pseudoinverse of $\mathbf{A}^{(3)}$. The TUCKER_ALS function relies on mean-squared-error minimization implemented in alternating least-square fashion [19]. I demonstrate performance of 3D TF-based SF BID on an experimental red–green–blue image shown in Fig. 1 with dimensions of 384 $\times$512 pixels i.e., $I_1=384$ and $I_2=512$. It has been recorded by digital camera in manually defocused mode. This image yields spatially invariant degradation that complies with fundamental property of the

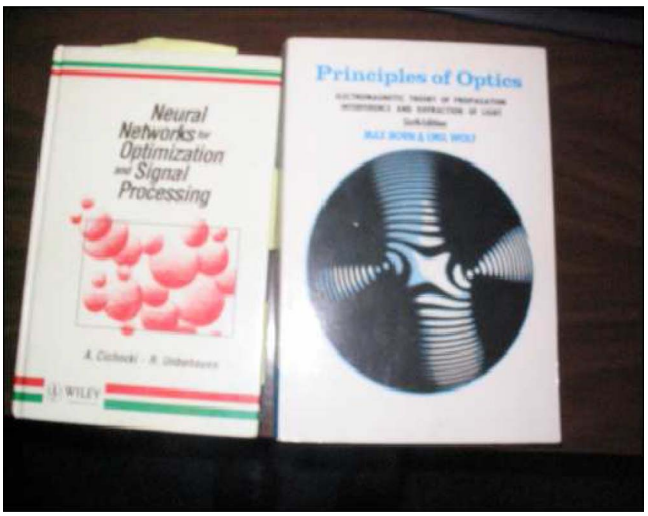

Fig. 1. (Color online) RGB experimental image obtained by digital camera in manually defocused mode. Images courtesy of (left) Wiley-Blackwell and (right) Cambridge University Press.

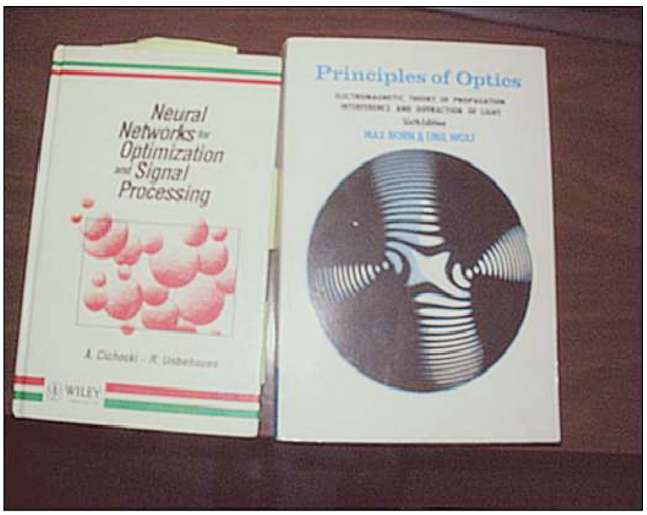

Fig. 2. (Color online) RGB image restored by 3D TF SF BID algorithm. Images courtesy of (left) Wiley-Blackwell and (right) Cambridge University Press.

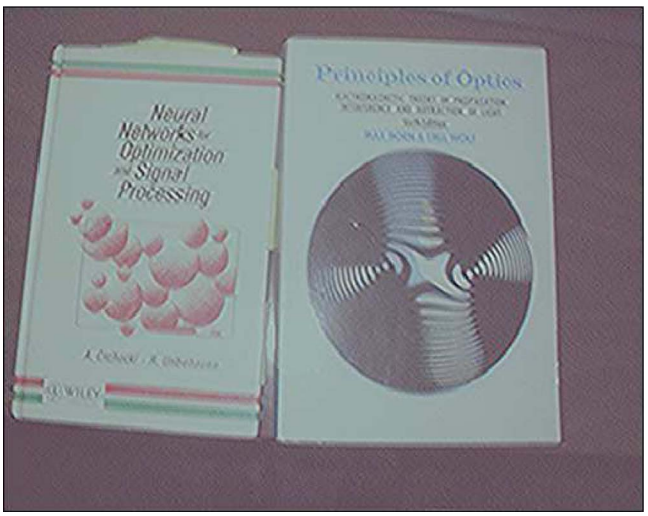

Fig. 3. (Color online) RGB image restored by WP SDICA BID algorithm [6]. Images courtesy of (left) Wiley-Blackwell and (right) Cambridge University Press.

convolution equation [Eq. (1)]. Thus it can be used for the proof-of-principle of the proposed SF BIF algorithm. The same image has been used previously in [4,6] in gray-scale version. Here, I use a color version (online) to demonstrate versatility of the 3D TF SF BID method. The color image is deconvolved by applying a described algorithm to each spectral image separately. Figure 2 shows the deconvolution result obtained by the 3D TF SF BID algorithm. This result was obtained by setting the number of latent variables in expression (4) to $J=5$. However, varying J between 3 and 16 yielded result of, in principle, the same quality. Figure 3 shows results obtained by the wavelet-packets-based subband decomposition ICA algorithm [6], where restoration errors are in part due to the image vectorization process and mainly due to the multiscale filtering necessary to satisfy the statistical independence constraint imposed on the latent variables in the linear mixture model [expression (5)]. Because of space limitation I did not carry out a comparative performance analysis between the TF SF BID method and blind Richardson–Lucy and NMF-based methods. However, based on results reported in [6] it might be concluded that TF-based method would compare favorably against them.

This work was partially supported through grant 098-0982903-2558 funded by the Ministry of Science, Education and Sports, Republic of Croatia.

References

1. M. R. Banham and A. K. Katsaggelos, IEEE Signal Process. Mag. **14**, 24 (1997).
2. D. Kundur and D. Hatzinakos, IEEE Signal Process. Mag. **13**, 43 (1996).
3. P. Campisi and K. Egiazarian, eds., *Blind Image Deconvolution* (CRC Press, 2007).
4. I. Kopriva, Opt. Lett. **30**, 3135 (2005).
5. A. Hyvärinen, J. Karhunen, and E. Oja, *Independent Component Analysis* (Wiley Interscience, 2001).
6. I. Kopriva, J. Opt. Soc. Am. A **24**, 973 (2007).
7. C. Yi-nan, J. Wei-qi, W. Ling-Xue, Z. Lei, and Y. Hongsheng, Opt. Commun. **282**, 786 (2009).
8. S. Umeyama, Scripta Technica, Electron. Comm. Jpn. Part 3 **84**, 1 (2001).
9. H. A. L. Kiers, J. Chemom. **14**, 105 (2000).
10. L. R. Tucker, Psychometrika **31**, 279 (1966).
11. J. D. Carrol and J. J. Chang, Psychometrika **35**, 283 (1970).
12. R. A. Harshman, in *UCLA Working Papers in Phonetics* (UCLA, 1970), Vol. 16, p. 1.
13. E. Acar and B. Yener, IEEE Trans. Knowl. Data Eng. **21**, 6 (2009).
14. J. B. Kruskal, Linear Algebr. Appl. **18**, 95 (1977).
15. N. D. Sidiropoulos and R. Bro, J. Chemom. **14**, 229 (2000).
16. N. Renard, S. Bourennane, and J. Blanc-Talon, IEEE Trans. Geosci. Remote Sens. Lett. **5**, 138 (2008).
17. N. Renard and S. Bourennane, IEEE Tras. Geosci. Remote Sens. **46**, 2407 (2008).
18. B. W. Bader and T. G. Kolda, *MATLAB Tensor Toolbox Version 2.2*, http://csmr.ca.sandia.gov/~tkolda/TensorToolbox.
19. L. De Lathauwer, B. De Moor, and J. Vandewalle, SIAM J. Matrix Anal. Appl. **21**, 1253 (2000).